

Evolution of Holographic Entanglement Entropy
after
Thermal and Electromagnetic Quenches

Tameem Albash, Clifford V. Johnson

*Department of Physics and Astronomy
University of Southern California
Los Angeles, CA 90089-0484, U.S.A.*

talbash, johnson1, [at] usc.edu

Abstract

We study the evolution and scaling of the entanglement entropy after two types of quenches for a 2+1 field theory, using a conjectured holographic technique for its computation. We study a thermal quench, dual to the addition of a shell of uncharged matter to four dimensional Anti-de Sitter (AdS_4) spacetime, and study the subsequent formation of a Schwarzschild black hole. We also study an electromagnetic quench, dual to the addition of a shell of charged sources to AdS_4 , following the subsequent formation of an extremal dyonic black hole. In these backgrounds we consider the entanglement entropy of two types of geometries, the infinite strip and the round disc, and find distinct behavior for each. Some of our findings naturally supply results analogous to observations made in the literature for lower dimensions, but we also uncover several new phenomena, such as (in some cases) a discontinuity in the time derivative of the entanglement entropy as it nears saturation, and for the electromagnetic quench, a logarithmic growth in the entanglement entropy with time for both the disc and strip, before settling to saturation. We briefly discuss the possible origin of the new phenomena in terms of the features of the conjectured dual field theory.

1 Introduction

The entanglement entropy of a quantum system has emerged as a useful probe in a number of fields. For example, the condensed matter community have recognized its utility as a diagnostic of phase transitions, especially in contexts where an analogue of a Landau–Ginsburg order parameter is either not accessible or available. The quantum information community employ it as a tool for assessing such things as the computational complexity of a system (see ref.[1] for a review). The quantum gravity community have used it to address important issues such as the entropy associated with a region of spacetime such as a black hole, where (for example) the important relation between the entropy of an excised region of spacetime (such as the interior of a black hole) and the area of the spacetime surrounding it can be motivated in terms of entanglement entropy (see *e.g.* ref.[2].) In such studies, it is very important to be able to extract information about how the entanglement entropy scales with the size of a given system, or evolves as a function of time.

Given a system, consider a region or subsystem which we can call \mathcal{A} , with the remaining part of the system denoted by \mathcal{B} . A definition of the entanglement entropy of \mathcal{A} with \mathcal{B} is given by:

$$S_{\mathcal{A}} = -\text{Tr}_{\mathcal{A}}(\rho_{\mathcal{A}} \ln \rho_{\mathcal{A}}) , \quad (1)$$

where $\rho_{\mathcal{A}}$ is the reduced density matrix of \mathcal{A} given by tracing over the degrees of freedom of \mathcal{B} , $\rho_{\mathcal{A}} = \text{Tr}_{\mathcal{B}}(\rho)$, where ρ is the density matrix of the system. When the system is in a pure state, *i.e.*, $\rho = |\Psi\rangle\langle\Psi|$, the entanglement entropy is a measure of the entanglement between the degrees of freedom in \mathcal{A} with those in \mathcal{B} . If the system starts in a pure state $|\Psi(0)\rangle$ and the evolution of the system is unitary, then the system at subsequent times is also a pure state $|\Psi(t)\rangle$, and so the evolution of the entanglement entropy describes the evolution of quantum entanglement in the system.

The evolution of entanglement entropy in a (1+1)–dimensional field theory after a quench was studied in ref. [3]. The system for $t < 0$ is in the ground state (with a mass gap), and at $t = 0$, the magnetic field is set to the critical point of the theory. Dividing the system into \mathcal{A} (a line segment of length ℓ) and \mathcal{B} (the rest), the analytical results for the system showed that the entanglement entropy grows linearly with time until it saturates at approximately $t = \ell/2$. Ref. [3] explained this as follows: at $t = 0$, the quench results in excitations that propagate to the left and to the right. Since the system before the quench had a mass gap, only excitations produced at around the same local region will be entangled. Contributions to the entanglement entropy occur when a left/right mover remains in region \mathcal{A} whereas the right/left mover is in region \mathcal{B} . So since at time t , the left–right pair are separated by a distance $2t$, saturation is reached when excitations produced at the center of \mathcal{A} reach \mathcal{B} which should be at $2t \simeq \ell$. It is of interest to study more such

systems and also to go beyond two dimensions. It is hard to make progress for many interacting field theories of interest, and so a search for powerful techniques from as broad a range of sources seems prudent. One such source of tools is the AdS/CFT correspondence[4, 5, 6].

A prescription for calculating the entanglement entropy [7] and its evolution [8] in the context of AdS/CFT provides a new way to calculate the entanglement entropy using geometrical techniques that are classical in spirit (for a review see ref.[9]). In an asymptotically Anti-de Sitter (AdS) geometry, consider a slice at constant AdS radial coordinate $z = a$. Recall that this defines the dual field theory (with one dimension fewer) as essentially residing on that slice in, in the presence of a UV cutoff set by the position of the slice. Sending the slice to the AdS boundary at infinity removes the cutoff (see ref. [10] for a review). On our $z = a$ slice, consider a region \mathcal{A} . Now find the minimal-area surface $\gamma_{\mathcal{A}}$ bounded by the perimeter of \mathcal{A} and that extends into the bulk of the geometry. Then the entanglement entropy of region \mathcal{A} with \mathcal{B} is given by:

$$S_{\mathcal{A}} = \frac{\text{Area}(\gamma_{\mathcal{A}})}{4G_{\text{N}}} , \quad (2)$$

where G_{N} is Newton's constant in the dual gravity theory. This prescription for the entropy coincides nicely with (1+1)-dimensional computations of the entanglement entropy, and has a natural generalization to higher dimensional theories. Note that there is no formal derivation of the prescription. Steps have been made, such as in refs. [11, 12], but they are not complete. However, there is lots of evidence for the proposal. See *e.g.*, refs.[13, 14, 15, 16, 17, 18]. A review of several of the issues can be found in ref.[9]. Further progress has been made recently in ref. [19]. Although there is no derivation available, in this paper we shall assume that this holographic prescription does give the correct result for the entanglement entropy in higher dimensions. Our results are interpreted in line with this. In particular, we find features that conform to expectations, and in addition we find new phenomena that we regard as predictions for the behavior of the field theory entanglement entropy.

Interesting recent papers, ref.[8, 20], presented a study of the time evolution of a (1+1)-dimensional system after a thermal quench, by working in the AdS₃ geometry dual to it. Since, *via* the AdS/CFT correspondence, a thermal state in the field theory is dual to a black hole on the gravity side[21], the authors started with AdS₃, perturbed it with a shell of matter, and then followed the subsequent formation of a black hole that took place, computing the entanglement entropy as a function of time using the above geometric prescription. They used the exact AdS₃ Vaidya metric to describe the formation process.

Their results confirmed a number of key features seen in the CFT computation of ref.[3]. In particular, the linear rise of the entanglement entropy with time, and the scaling of the saturation time with the size of the system showing that the effective propagation speed of the entanglement

was the speed of light. (Among the many interesting features of such computations is the fact that the minimal surfaces involved must probe the region *behind* the apparent black hole horizon.)

The goal of the work we report on was primarily two-fold. First, we wished to examine the question of higher dimensions, and so we used an AdS_4 setting, relevant to the study of dual 2+1 dimensional field theory. The question of how the entropy evolves in time and scales with the size of the system can be examined, and the physics of the growth of entanglement due to the propagation of quanta ought to be more interesting since there are more shapes available for region \mathcal{A} . We examine the physics of the infinite strip and the round disc and indeed see rather interesting physics to compare and contrast, again following an evolution after a thermal quench modeled by a four dimensional Vaidya metric for gravitational collapse. A second issue we wished to address was how to do a different, non-thermal, type of quench in this AdS/CFT context, and to compare our results for it to the thermal case. We constructed a non-thermal quench by exciting electromagnetic sectors instead. There is a natural $U(1)$ sector to which the physics couples and so starting with pure AdS_4 we study and evolution of a shell (using a charged generalization of the Vaidya metric) which ultimately forms a zero temperature state at late times: an extremal black hole. So the quench is non-thermal, and the excitation in our new example is either by an external magnetic field or by a chemical potential for charge density, or an admixture of the two that can be freely dialed up using the four dimensional electric-magnetic duality of the four dimensional gravity system.

In section 2 we give the general framework in which we are working, setting out our notation and the general form of the computation. We illustrate our methods by working out results for some familiar static geometries, re-deriving old results and adding some new ones (those for the case of extremal dyonic black holes). Section 3 presents our new results for the thermal quench in higher dimensions, where we notice several new features of the physics, including a kink in the time evolution of the entropy as it heads to saturation, for large enough system size. The case of the disc and the strip are thoroughly examined and contrasted. Section 4 presents the electromagnetic quench, discussing again many new features seen for the case of the disc and the strip. We conclude in section 5, and there is a brief appendix about the unitarity of the quench evolutions.

2 General Framework

In this section we present the setting for our computations of minimal surfaces in asymptotically AdS_4 geometries. We will present some examples of static test geometries in section 2.3, with some familiar results and some new ones. This will allow us to set up notation and orient the discussion.

2.1 Gravity Background

We consider the Einstein–Maxwell action:

$$S = \frac{1}{16\pi G_N} \int d^4x \sqrt{-G} (\mathcal{R} - 2\Lambda - F^2) + S_{ext} , \quad (3)$$

where the cosmological constant $\Lambda = -3/R^2$ sets a length scale R , and we will present the external sources we are interested in shortly. The equations of motion are given by:

$$\mathcal{R}_{\mu\nu} - \frac{1}{2}G_{\mu\nu} (\mathcal{R} - 2\Lambda - F^2) - 2F_{\mu\lambda}F_{\nu}{}^{\lambda} = 8\pi G_4 T_{\mu\nu}^{(\text{ext})} , \quad (4)$$

$$\frac{1}{\sqrt{-G}} \partial_{\mu} (\sqrt{-G} F^{\mu\nu}) = 4\pi G_4 J_{(\text{e-ext})}^{\nu} . \quad (5)$$

We consider a solution to these equations of the form [22]:

$$ds^2 = -V(r, v)dv^2 + 2drdv + \frac{r^2}{R^2}d\vec{x}^2 , \quad (6)$$

$$V(r, v) = \frac{r^2}{R^2} - \frac{2m(v)}{r} + \frac{q_e(v)^2 + q_m(v)^2}{r^2} , \quad (7)$$

$$F_{rv} = \frac{q_e(v)}{r^2} , \quad F_{xy} = \frac{q_m(v)}{R^2} , \quad (8)$$

which correspond to having sources given by:

$$4\pi G_4 J_{\text{e-ext}}^{\mu} = \frac{\dot{q}_e}{r^2} \delta^{\mu\nu} , \quad 8\pi G_4 T_{\mu\nu}^{\text{ext}} = -\frac{2}{r^3} (q_e \dot{q}_e + q_m \dot{q}_m - r\dot{m}) \delta_{\mu\nu} \delta_{vv} . \quad (9)$$

This solution is a generalization of the Vaidya metric [23, 24]. Note that in terms of the Hodge dual field, we can write:

$$\frac{1}{\sqrt{-G}} \partial_{\mu} (\sqrt{-G} (*F)^{\mu\nu}) = 4\pi G_4 J_{(\text{m-ext})}^{\nu} , \quad 4\pi G_4 J_{(\text{m-ext})}^{\mu} = \frac{\dot{q}_m}{r^2} \delta^{\mu\nu} . \quad (10)$$

Also note that $(m(v), q_e(v), q_m(v))$ have dimensions of length. It is convenient to work in terms of a coordinate z :

$$z = \frac{R^2}{r} , \quad (11)$$

such that we can write the metric as:

$$ds^2 = \frac{R^2}{z^2} (-f(z, v)dv^2 - 2dzdv + d\vec{x}^2) , \quad f(z, v) = 1 - \frac{2m(v)}{R^4} z^3 + \frac{q_e(v)^2 + q_m(v)^2}{R^6} z^4 . \quad (12)$$

The time coordinate t of the dual field theory emerges (near the AdS boundary) as:

$$v \sim t - z . \quad (13)$$

2.2 Entanglement Entropy for the Strip and Disc

2.2.1 The Strip

We first consider calculating the entanglement entropy of an infinite strip, which we denote as region \mathcal{A} in the dual field theory. We consider the area of a two-dimensional surface $\gamma_{\mathcal{A}}$ that extends into the bulk that is joined to the boundary of \mathcal{A} . We depict this in figure 1(a).

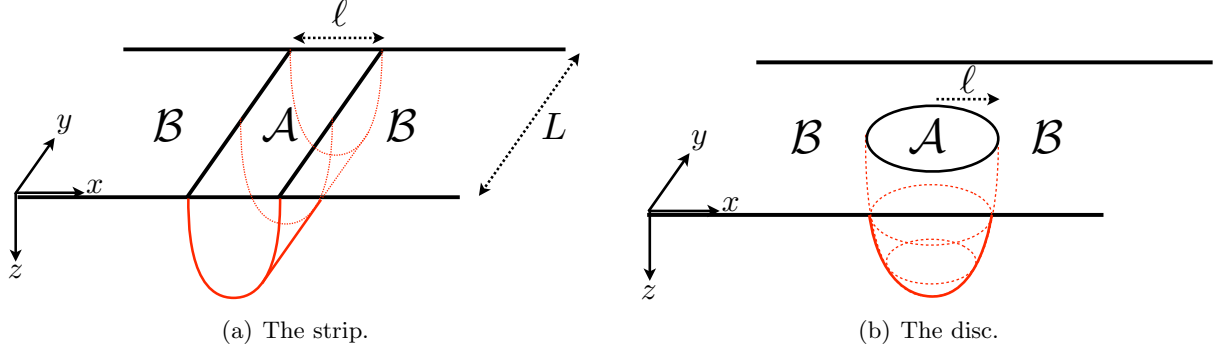


Figure 1: Diagrams of the two shapes we will consider for region \mathcal{A} .

We parameterize the surface with coordinates:

$$\xi^1 = x, \quad \xi^2 = y, \quad (14)$$

At $z = \epsilon$, very near the AdS boundary, (ϵ is the UV cutoff of the dual field theory), the region \mathcal{A} will be chosen such that:

$$\mathcal{A} := x \in \left(-\frac{\ell}{2}, \frac{\ell}{2}\right), \quad y \in (0, L). \quad (15)$$

with L taken to infinity. The area of this surface is given by:

$$\text{Area}(\gamma_{\mathcal{A}}) = L \int_{-\ell/2}^{\ell/2} dx \sqrt{h}, \quad (16)$$

where $h_{\alpha\beta}$ is the induced metric on the surface given by:

$$h_{\alpha\beta} = G_{\mu\nu} \frac{dx^\mu}{d\xi^\alpha} \frac{dx^\nu}{d\xi^\beta}. \quad (17)$$

By the symmetry of the strip, we consider an ansatz of the following form for the embedding profile of $\gamma_{\mathcal{A}}$:

$$v \equiv v(x), \quad z \equiv z(x), \quad z(\pm\ell/2) = \epsilon, \quad v(\pm\ell/2) = t - \epsilon, \quad (18)$$

such that the area is given by:

$$\text{Area}(\gamma_{\mathcal{A}}) = LR^2 \int_{-\ell/2}^{\ell/2} dx \frac{\sqrt{1 - f(v, z)v'(x)^2 - 2v'(x)z'(x)}}{z(x)^2}. \quad (19)$$

We denote the integrand in equation (19) as the Lagrangian \mathcal{L} of our system. Since there is no explicit x dependence, a constant of the motion is the Hamiltonian \mathcal{H} (if we think of the coordinate x as a time coordinate),

$$\mathcal{H} = \mathcal{L} - v'(x) \frac{\delta \mathcal{L}}{\delta v'(x)} - z'(x) \frac{\delta \mathcal{L}}{\delta z'(x)} = \frac{1}{z(x)^2 \sqrt{1 - f(v, z) v'(x)^2 - 2v'(x) z'(x)}} . \quad (20)$$

By the symmetry of the problem, and by choice of origin of x , we look for a turning point at $x = 0$, and at this turning point, we have:

$$v'(0) = z'(0) = 0 , \quad z(0) = z_* , \quad v(0) = v_* . \quad (21)$$

Therefore, we have the result that $\mathcal{H} = z_*^{-2}$. Using this result and equation (20), we can write the following conservation equation:

$$1 - f(v, z) v'(x)^2 - 2v'(x) z'(x) = \frac{z_*^4}{z(x)^4} . \quad (22)$$

By taking the x -derivative of this equation, and substituting for $z''(x)$ in the two equations of motion, we get a single equation:

$$-4 + 4f(v, z) v'(x)^2 + 8v'(x) z'(x) + 2z(x) v''(x) - z(x) v'(x)^2 \partial_z f(v, z) = 0 . \quad (23)$$

Similarly, if we took the x -derivative of the conservation equation, and substituting for $v''(x)$ in the two equations of motion, we get a single equation:

$$4f(v, z)^2 v'(x)^2 - f(v, z) (4 - 8v'(x) z'(x) + z(x) v'(x)^2 \partial_z f(v, z)) - z(x) (2z''(x) + v'(x) (2z'(x) \partial_z f(v, z) + v'(x) \partial_v f(v, z))) = 0 . \quad (24)$$

The “on-shell” area is now given simply by:

$$\text{Area}(\gamma_{\mathcal{A}}) = 2LR^2 \int_0^{\ell/2} dx \frac{z_*^2}{z(x)^4} . \quad (25)$$

2.2.2 The Disc

We may now consider the disc. We consider a disc of radius ℓ , and take the two dimensional surface $\gamma_{\mathcal{A}}$, which we depict in figure 1(b), to be parameterized by:

$$\xi^1 = r , \quad \xi^2 = \phi . \quad (26)$$

By the rotational symmetry of the problem, we can consider an ansatz of the form:

$$z \equiv z(r) , \quad v \equiv v(r) . \quad (27)$$

This gives for the area:

$$\text{Area}(\gamma_{\mathcal{A}}) = 2\pi R^2 \int_0^\ell dr \frac{r}{z(r)^2} \sqrt{1 - f(v, z)v'(r)^2 - 2v'(r)z'(r)} . \quad (28)$$

Because there is an explicit r appearing in the Lagrangian, we do not have a conserved quantity associated with the disc as we did for the strip. However, by the symmetry of the problem we again must have:

$$z'(0) = v'(0) = 0 . \quad (29)$$

The general equations of motion derived from the extremizing of the area in equation (28) are straightforward to derive. We do not write them here, in general, as they are rather long. Later, specific cases will be written.

2.3 Static Examples

Following are computations for the entanglement entropy for three static spacetime examples. In each case we present the results for the strip and the disc.

2.3.1 Pure AdS₄

Let us calculate the entanglement entropy for pure AdS₄ [7]. This means taking $f(v, z) = 1$. Although it is simpler to exchange v for t , let us proceed with the given choice of coordinates. A solution to the equations of motion (23) and (24) is simply to take:

$$v'(x) = -z'(x) . \quad (30)$$

Then the conservation equation (22) allows us to write:

$$\frac{dz}{dx} = \pm \sqrt{\frac{z_*^4}{z^4} - 1} , \quad (31)$$

where the plus sign is taken for $x < 0$ and the minus sign is taken for $x > 0$. We can use this result to find a relationship between z_* and ℓ by simply integrating equation (31):

$$\frac{\ell}{2} = \int_\epsilon^{z_*} dz \left(\frac{z_*^4}{z^4} - 1 \right)^{-1/2} . \quad (32)$$

Changing coordinates to $u = z^4/z_*^4$, we can write this integral in a more convenient form:

$$\frac{\ell}{2} = \frac{z_*}{4} \int_{\frac{\epsilon^4}{z_*^4}}^1 du u^{-3/4} (1-u)^{-1/2} = B\left(\frac{1}{4}, \frac{1}{2}\right) - B\left(\frac{\epsilon^4}{z_*^4}; \frac{1}{4}, \frac{1}{2}\right) , \quad (33)$$

where $B(a, b)$ is the Euler beta function, and $B(x; a, b)$ is the incomplete beta function. In this expression, we can take $\epsilon \rightarrow 0$ without encountering any divergences, so our result is simply:

$$\frac{\ell}{2} = z_* \frac{\sqrt{\pi}\Gamma(3/4)}{\Gamma(1/4)}. \quad (34)$$

Using the same procedures, we can write our “on-shell” area as:

$$\text{Area}(\gamma_{\mathcal{A}}) = \frac{2LR^2}{z_*^2} \int_a^{z_*} dz \frac{z_*^2}{z^2} \left(1 - \frac{z^4}{z_*^4}\right)^{-1/2}. \quad (35)$$

Changing coordinates to $u = z^4/z_*^4$, we can write this integral in a convenient form:

$$\text{Area}(\gamma_{\mathcal{A}}) = \frac{2LR^2}{4z_*} \int_{\frac{\epsilon^4}{z_*^4}}^1 du u^{-5/4} (1-u)^{-1/2} = \frac{2RL}{4z_*} \left(B\left(-\frac{1}{4}, \frac{1}{2}\right) - B\left(\frac{\epsilon^4}{z_*^4}; -\frac{1}{4}, \frac{1}{2}\right) \right). \quad (36)$$

Expanding our expression for small ϵ (in order to capture the divergent contribution from our UV cutoff), we get our final result for the area [7]:

$$\text{Area}(\gamma_{\mathcal{A}}) = \frac{2R^2L}{\epsilon} + \frac{R^2L}{2z_*} \frac{\sqrt{\pi}\Gamma(-1/4)}{\Gamma(1/4)} = 2RL \left(\frac{R}{\epsilon} + \frac{R}{2\ell} \frac{\pi\Gamma(-1/4)\Gamma(3/4)}{\Gamma(1/4)^2} \right). \quad (37)$$

The divergent first term is proportional to the boundary of \mathcal{A} . We will be generally interested in the finite contribution to the entropy given by the second term, which we denote s :

$$s = \frac{1}{4G_{\text{N}}} \left(\text{Area}(\gamma_{\mathcal{A}}) - \frac{2R^2L}{\epsilon} \right) \quad (38)$$

We will work in terms of the rescaled finite entropy \tilde{s} , a function of terms of the dimensionless length $\tilde{\ell} = \ell/R$,

$$\tilde{s} = \frac{4G_{\text{N}}}{2RL} s, \quad (39)$$

which we plot in figure 2.

We can proceed in a similar fashion for the disc. A solution to the equations of motion is to take the result of equation (30), which then gives us one equation for $z(r)$:

$$2r(1 + z'(r)^2) + z(r)(z'(r) + z'(r)^3 + rz''(r)) = 0. \quad (40)$$

A solution to this equation is:

$$z(r)^2 + r^2 = \ell^2, \quad (41)$$

which describes the extremal surface as a half-sphere (of radius ℓ) in the bulk. The area is given by:

$$\text{Area}(\gamma_{\mathcal{A}}) = 2\pi R^2 \ell \int_0^\ell dr \frac{r}{z(r)^3}. \quad (42)$$

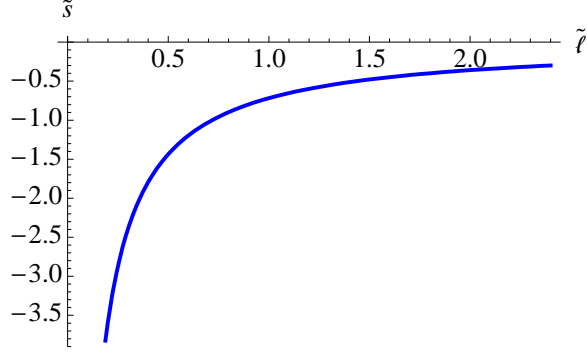


Figure 2: The finite contribution to the entanglement entropy as a function of $\tilde{\ell} = \ell/R$ in the pure AdS₄ background.

We use the fact that $dz = -rdr/z$ and $z_* = \ell$, and we change coordinates to $y = z/\ell$ to write the integral as:

$$\text{Area}(\gamma_{\mathcal{A}}) = 2\pi R^2 \int_{\epsilon/\ell}^1 \frac{dy}{y^2} = 2\pi R^2 \left(\frac{\ell}{\epsilon} - 1 \right). \quad (43)$$

If we define the finite contribution to the entropy by:

$$s = \frac{1}{4G_{\text{N}}} \left(\text{Area}(\gamma_{\mathcal{A}}) - \frac{2\pi R^2 \ell}{\epsilon} \right), \quad (44)$$

and consider the rescaled entropy \tilde{s}

$$\tilde{s} \equiv \frac{4G_{\text{N}}}{2\pi R^2} s, \quad (45)$$

then we find that $\tilde{s} = -1$. Note in particular that there is no dependence on $\tilde{\ell}$, the size of the disc[7]. We emphasize that this is a significant difference from the strip and is a simple result of scale invariance in the theory when a shape that preserves conformal invariance on the boundary is taken for \mathcal{A} .

2.3.2 AdS₄–Schwarzschild

To study the case of AdS₄–Schwarzschild[7], we take $f(v, z) = 1 - 2mz^3/R^4$. In this geometry, the event horizon is located at a radial distance z_0 given by:

$$z_0 = \left(\frac{2m}{R^4} \right)^{-1/3}. \quad (46)$$

We once again start with the strip. A solution to the equations of motion is to take:

$$v(x) = t + g(z(x)), \quad \partial_{z(x)} g(z(x)) = -f(z(x))^{-1}. \quad (47)$$

The remaining equation of motion is given by:

$$-2z(x)z''(x) + z'(x)^2 \left(-4 + z(x) \frac{\partial_{z(x)} f(z(x))}{f(z(x))} \right) - 4f(z) = 0. \quad (48)$$

The conservation equation is now given by:

$$1 + \frac{z'(x)^2}{f(z(x))} = \frac{z_*^4}{z(x)^4}, \quad (49)$$

which allows us to write:

$$\frac{dz}{dx} = \pm \sqrt{f(z(x)) \left(\frac{z_*^4}{z(x)^4} - 1 \right)}. \quad (50)$$

In turn, the area can be written as:

$$\text{Area}(\gamma_{\mathcal{A}}) = \frac{2LR^2}{z_*^2} \int_{\epsilon}^{z_*} dz \frac{z_*^2}{z^2} \left(f(z) \left(1 - \frac{z^4}{z_*^4} \right) \right)^{-1/2}, \quad (51)$$

and the length is given by:

$$\frac{\ell}{2} = \int_0^{z_*} dz \frac{z^2}{z_*^2} \left(f(z) \left(1 - \frac{z^4}{z_*^4} \right) \right)^{-1/2}. \quad (52)$$

It is convenient at this point to define dimensionless variables:

$$\tilde{z} = \frac{z}{z_0}, \quad \tilde{x} = \frac{x}{z_0}, \quad (53)$$

such that:

$$\text{Area}(\gamma_{\mathcal{A}}) = \frac{2LR^2}{z_0} \int_{\tilde{\epsilon}}^{\tilde{z}_*} d\tilde{z} \tilde{z}^{-2} \left((1 - \tilde{z}^3) \left(1 - \frac{\tilde{z}^4}{\tilde{z}_*^4} \right) \right)^{-1/2}, \quad (54)$$

and

$$\frac{\tilde{\ell}}{2} = \int_0^{\tilde{z}_*} d\tilde{z} \frac{\tilde{z}^2}{\tilde{z}_*^2} \left((1 - \tilde{z}^3) \left(1 - \frac{\tilde{z}^4}{\tilde{z}_*^4} \right) \right)^{-1/2}. \quad (55)$$

Since there is no analytic expression for the area, we wish to express the finite contribution to the entanglement in a way that is consistent with our pure AdS₄ result using equation (38). Furthermore, we can define a rescaled entropy \tilde{s} as in equation (39):

$$\tilde{s} = \frac{R}{z_0} \left[\int_{\tilde{\epsilon}}^{\tilde{z}_*} d\tilde{z} \tilde{z}^{-2} \left((1 - \tilde{z}^3) \left(1 - \frac{\tilde{z}^4}{\tilde{z}_*^4} \right) \right)^{-1/2} - \frac{1}{\tilde{\epsilon}} \right] \quad (56)$$

We present a plot of this finite contribution to the area in figure 3. In particular, note that for large $\tilde{\ell}$, the result for $z_0 \tilde{s}/R$ scales as $\tilde{\ell}/2$ which is exactly what is needed to recover the entropy–area law, *i.e.*:

$$(4G_{\text{N}})s \sim \frac{R^2}{z_0^2} L\ell, \quad \text{for } \ell/z_0 \text{ large}. \quad (57)$$

We can perform a similar computation for the disc. The area can be written as:

$$\text{Area}(\gamma_{\mathcal{A}}) = 2\pi R^2 \int_0^{\tilde{\ell}} d\tilde{r} \frac{\tilde{r}}{\tilde{z}^2} \sqrt{1 + \frac{\tilde{z}'(\tilde{r})^2}{1 - \tilde{z}^3}}. \quad (58)$$

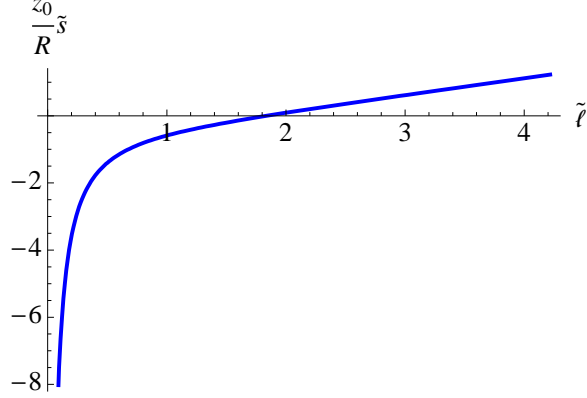


Figure 3: The finite contribution to the entanglement entropy for the strip as a function of $\tilde{\ell} = \ell/z_0$ in the AdS_4 -Schwarzschild background.

We write the finite contribution to the entropy s as in equation (44), and we write the rescaled entropy \tilde{s} as in equation (45):

$$\tilde{s} = \int_0^{\tilde{\ell}} d\tilde{r} \frac{\tilde{r}}{\tilde{z}^2} \sqrt{1 + \frac{\tilde{z}'(\tilde{r})^2}{1 - \tilde{z}^3}} - \frac{\tilde{\ell}}{\tilde{\epsilon}}. \quad (59)$$

We present the behavior of the area in figure 4. We see that for small $\tilde{\ell}$, the contribution matches that of pure AdS_4 , as the surface remains close to the AdS boundary. For large $\tilde{\ell}$, the behavior of the area is quadratic in $\tilde{\ell}$ as is to be expected, since most of the contribution will come from the surface behaving as a disc at the event horizon. Again we find that for large $\tilde{\ell}$, the entropy \tilde{s} scales

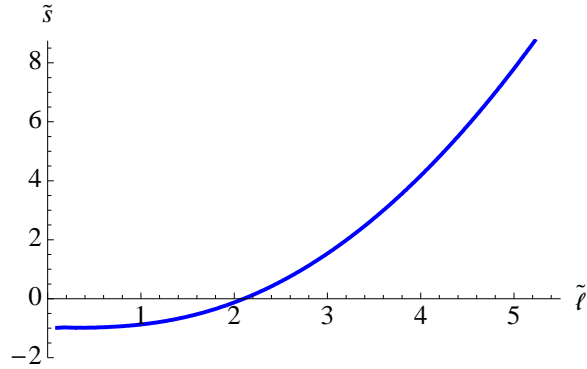


Figure 4: The finite contribution to the entanglement entropy for the disc as a function of ℓ/z_0 in the AdS_4 -Schwarzschild background.

as $\tilde{\ell}^2/2$, which again recovers the entropy–area law:

$$(4G_{\text{N}})s \sim \frac{R^2}{z_0^2} \pi \ell^2, \text{ for } \ell/z_0 \text{ large}. \quad (60)$$

2.3.3 Extremal AdS₄–Dyonic

We now consider the extremal AdS₄ dyonic black hole. The entanglement entropy for this static case has not been studied (as far as we know) in the literature, and so the results are new. This is a useful preparatory computation for the electromagnetic quench we will perform in a later section.

We have:

$$f(z) = 1 - 4 \left(\frac{z}{z_0} \right)^3 + 3 \left(\frac{z}{z_0} \right)^4, \quad (61)$$

where we have used that:

$$Q^2 = q_e^2 + q_m^2 = \frac{3m}{2z_0} R^2, \quad z_0^3 = \frac{2R^4}{m}. \quad (62)$$

Equations (47), (48), (49), (50), (51), and (52) remain unchanged. We can define the finite part of the entropy using equation (38) and the rescaled entropy using equation (39). We present the finite contribution to the area in figure 5. As in the case of the Schwarzschild black hole, for large $\tilde{\ell}$ we recover the entropy–area law with a linear dependence in $\tilde{\ell}$. Performing a similar calculation

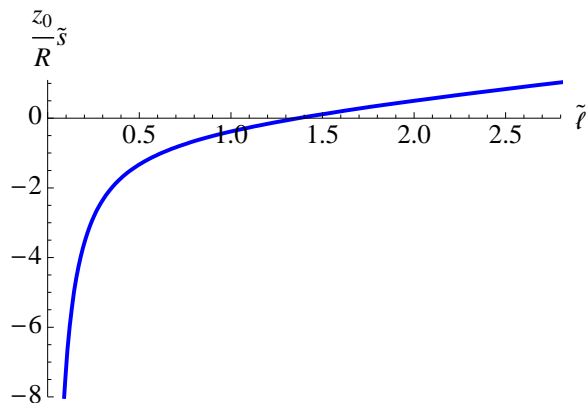


Figure 5: The finite contribution to the entanglement entropy for the disc as a function of ℓ/R in the AdS₄ Dyonic black hole background.

for the disc gives the results in figure 6. We see again that for $\tilde{\ell}$ large, the behavior is such that we recover the entropy–area law, with a quadratic dependence in $\tilde{\ell}$.

A new feature of this background is that the area integral exhibits a logarithmic divergence as z_* approaches the event horizon. This is a simple result of the fact that the event horizon has a double zero. This feature will play a role in the evolution of our electromagnetic quench discussed later. To see this more explicitly, as an extreme example, consider the embedding with $z_* = z_0$. This embedding consists of a piece that extends along the event horizon, and then two pieces that extend from the AdS boundary at $x = \pm\ell/2$ (for the strip) to the event horizon. We present a depiction of this embedding in figure 7. The contribution to the area of the pieces that fall towards

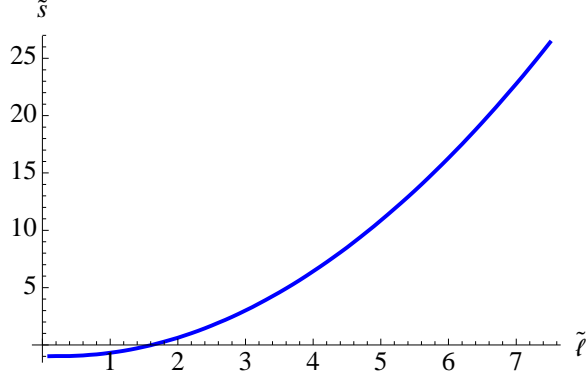


Figure 6: The finite contribution to the entanglement entropy for the disc as a function of ℓ/R in the AdS₄ Dyonic black hole background.

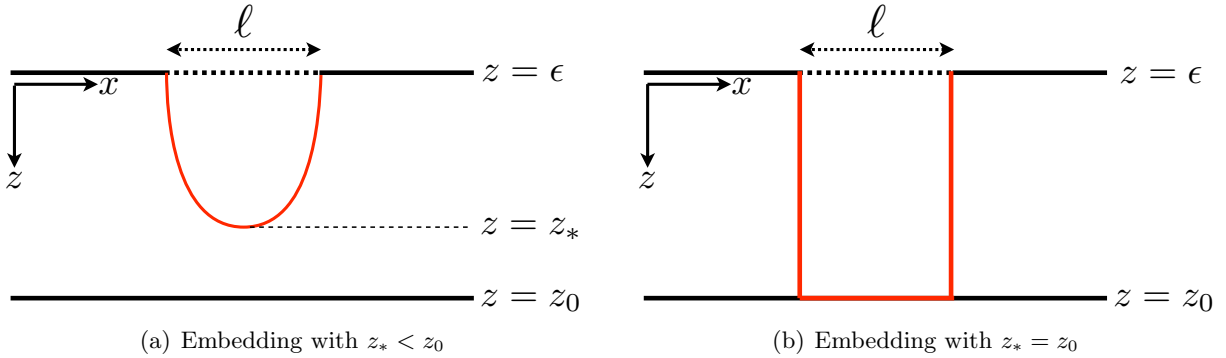


Figure 7: Diagrams of the two types of embeddings in the presence of a black hole.

the event horizon is given by:

$$\text{Area}(\gamma_{\mathcal{A}}) = 2L \int_{\epsilon}^{z_0} \frac{R^2}{z^2} f(z)^{-1/2} . \quad (63)$$

Near the event horizon, we can write:

$$f(z \rightarrow z_0) = \frac{6}{z_0^2} (z_0 - z)^2 , \quad (64)$$

and so we have:

$$\text{Area}(\gamma_{\mathcal{A}}) \sim \int^{\epsilon} \frac{dz}{z_0 - z} , \quad (65)$$

which contributes a logarithmic divergence to the area.

3 The Thermal Quench

We begin by extending the very interesting work of refs. [8, 20] to one dimension higher, performing a thermal quench. We will get several new results, and contrast them with several more new results

that we obtain for a new, electromagnetic, holographic quench in a later section. The idea of the holographic quench studied in refs.[8, 20] (see also ref.[25]) is that the system is simply AdS at early times, and then at some later time it is strongly perturbed by a shell of collapsing null dust, which subsequently forms a Schwarzschild black hole at late times, representing a thermal state in the holographically dual theory[21]. The point of the exercise is to study the evolution of the entanglement entropy over time after the quench¹. Generically, it saturates after a characteristic time. In 1+1 dimensions the behaviour is rather simple, with a linear rise in the entropy followed by a distinct leveling off to saturation, as observed in a magnetically quenched system in ref.[3], and a thermally quenched system using holographic duality to asymptotically AdS₃ geometries in refs.[8, 20]. The slope of the line reflects the fact that the effects of the quench propagate at the speed of light in the single dimension available. We shall see more complicated possibilities in higher dimensions and in the next section when we do an electromagnetic (non-thermal) quench.

To achieve the quench, we consider:

$$f(v, z) = 1 - \left(\frac{z}{z_0(v)} \right)^3, \quad m(v) = z_0(v)^{-3}. \quad (66)$$

and take the following functional form for $z_0(v)$:

$$z_0(v) = z_\infty \left(\frac{1 + \tanh(v/v_0)}{2} \right)^{-1/3}. \quad (67)$$

This form for $z_0(v)$ is such that the background is pure AdS₄ in the infinite past and an AdS₄-Schwarzschild black hole in the infinite future. See figure 8. The parameter z_∞ can be thought of

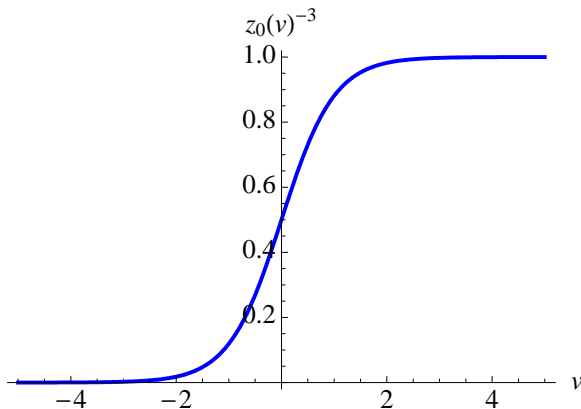


Figure 8: The shape of the mass function $m(v)$, generating the quench from pure AdS₄ to a finite mass black hole.

¹This evolution is indeed unitary, as it ought to be [20]. See the appendix for some clarifying comments on that issue. We thank E. Lopez for a discussion on this point.

as being related to the final temperature of the background at late times:

$$T = \frac{3}{4\pi} z_\infty^{-1} , \quad (68)$$

and the parameter v_0 is related to the time over which the quench occurs. As in the case of the static AdS₄–Schwarzschild black hole, we rescale z and x by z_∞ to define dimensionless coordinates \tilde{z} and \tilde{x} . We proceed to solve equations (23) and (24) numerically using a shooting method with the following initial conditions:

$$\tilde{v}'(0) = \tilde{z}'(0) = 0 , \quad \tilde{z}(0) = \tilde{z}_* , \quad \tilde{v}(0) = \tilde{v}_* . \quad (69)$$

Near the AdS boundary (*i.e.* when $\tilde{x} = \tilde{\ell}/2$ for the strip or when $\tilde{r} = \tilde{\ell}$ for the disc), we extract the following information:

$$\tilde{z}(\tilde{\ell}/2) = \tilde{\epsilon} , \quad \tilde{v}(\tilde{\ell}/2) = \tilde{t} - \tilde{\epsilon} , \quad (70)$$

Because of the form we choose for our quench, the quench starts at approximately $\tilde{t} \approx -2\tilde{v}_0$.

3.1 The Strip

After the rescaling, the area of the surface given in equation (25) is given by:

$$\text{Area}(\gamma_{\mathcal{A}}) = \frac{2LR^2}{z_\infty} \int_0^{\tilde{\ell}/2} d\tilde{x} \frac{\tilde{z}_*^2}{\tilde{z}(\tilde{x})^4} . \quad (71)$$

We define the finite contribution to the entanglement entropy s as in equation (38), but we modify our definition of the rescaled entropy from equation (39) by subtracting the pure AdS₄ result we have found in section 2.3.1:

$$\tilde{s} = \frac{R}{z_\infty} \left[\int_0^{\tilde{\ell}/2} d\tilde{x} \frac{\tilde{z}_*^2}{\tilde{z}(\tilde{x})^4} - \frac{1}{\tilde{\epsilon}} - \frac{\pi}{2\tilde{\ell}} \frac{\Gamma(-1/4)\Gamma(3/4)}{\Gamma(1/4)^2} \right] , \quad (72)$$

and with this subtraction we have chosen that the entanglement entropy \tilde{s} starts at zero in the infinite past. We present some results in figure 9, showing the evolution for a range of quench speeds, set by \tilde{v}_0 . We see that the curves almost perfectly overlap when \tilde{v}_0 is small enough, except in the region before saturation is reached, where the curve with smaller \tilde{v}_0 appears to be sharper. The invariance of the early evolution suggests that regardless of how fast the quench is done, the early evolution is dictated by a time constant that is only dependent on the details of the plasma described by the dual 2+1 dimensional field theory. This behavior was also observed in refs.[8, 20] for one dimension fewer. Notice that for large \tilde{v}_0 , the evolution of the entropy appears to follow the evolution of the quench rather closely. For short quenches the system relaxes to its new state more slowly.

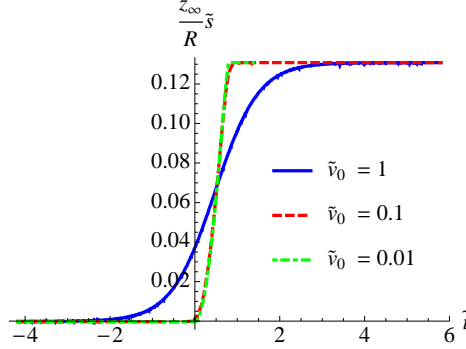


Figure 9: The evolution of \tilde{s} for different quench speeds for $\tilde{\ell} = 1$.

Exploring the behavior as we change the strip width $\tilde{\ell}$, we note several things. First, the early evolution appears to be independent of (or only weakly dependent on) $\tilde{\ell}$. This can be understood from the geometry of the strip. As ℓ changes, the area at the boundary of \mathcal{A} does not change, so the initial propagation of excitations from region \mathcal{A} to region \mathcal{B} , contributing to the entanglement, is not affected by the strip width. Second, we see the appearance of a new phenomenon, the appearance of a swallow tail. See figure 10. The swallow tail is a feature of our numerical method for searching for minimal area solutions with a given UV and IR boundary condition at a given time \tilde{t} . The method reveals the presence of multiple (at times up to three) solutions to the problem for a given time. By studying figure 11(a), we see that the multiplicity corresponds to the presence of solutions that have a \tilde{z}_* below and above the apparent horizon. The solution is always the one with the lowest area, and therefore the transition leads to a kink in the entropy dependence on time. Figure 11(b) explicitly shows the three embeddings at the transition; the transition is from an embedding with several sharp features to a smooth one.

This kink in the evolution of the entanglement entropy is a striking new feature in time evolution. Notice that the branch of solutions joined on to at late times are ones for which the turning point of the minimal surfaces, \tilde{z}_* , is well above the final horizon, \tilde{z}_∞ , giving an \tilde{s} which is essentially the saturated late time value. In other words, the entropy reaches saturation and then abruptly flattens out for large enough strip size $\tilde{\ell}$. For smaller strip size, the transition is also fast, but not so fast as to have a discontinuity in the derivative. Since the rate of approach to saturation is not strongly dependent on the region size $\tilde{\ell}$, while the saturation value itself depends on $\tilde{\ell}$, it is reasonable to expect that upon nearing saturation, the evolution turns over and flattens out toward the saturation value. In cases where the saturation value increases fast enough with $\tilde{\ell}$ (linearly with $\tilde{\ell}$ for the strip) while the rate of approach remains constant or weakly dependent on $\tilde{\ell}$, this turnover will be more pronounced for large enough $\tilde{\ell}$. In these large N systems we are studying, this is, we

presume, the role of the kink, which as we have seen appears for large enough $\tilde{\ell}$. We expect that the sharp transition would be softened by $1/N$ corrections upon leaving the gravity approximation.

Our results suggest that the picture proposed in ref. [3], which arose in the 1+1 dimensional case, needs modification here. In their picture, the entropy is discussed in terms of left and right moving pairs in the field theory. Saturation occurs once all pairs have had enough time to have traveled a distance of order the size of the interval. For our higher dimensional geometries we see saturation before all the analogous pairs are separated enough (here for the strip, for example, there are directions for which pairs can travel for extremely long times before leaving the strip). This suggests that the entanglement entropy is not built from simple pairwise contributions for the higher dimensional cases under consideration here. The bulk of the contributions from those longer-traveling quanta must have been already accounted for, and the system nears saturation without them having departed the starting region.

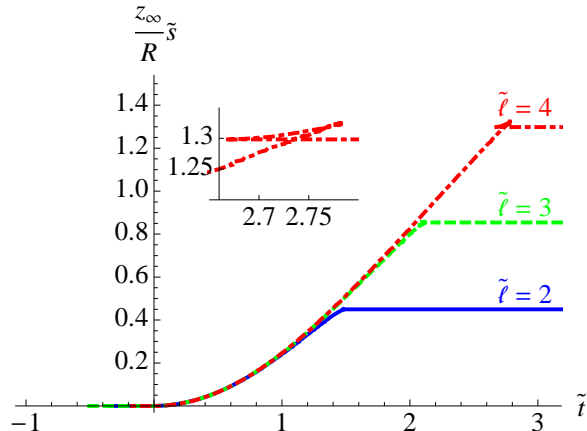


Figure 10: Results for thermal quench for $\tilde{v}_0 = 0.01$.

Turning to the intermediate time region where the entanglement entropy grows rapidly, we show in figure 12) the behavior of the saturation time for various $\tilde{\ell}$. Near $\tilde{\ell} = 0$, the best fit line has slope 0.77, yet for much larger $\tilde{\ell}$, the slope is closer to 0.65 (Note that there is some flexibility in this number depending on how one defines the edges of the growth period to extract the saturation time t_{sat}). Interestingly, therefore, it seems that the saturation rate for the thermal case grows faster for larger ℓ . This is traceable to the early time behaviour of the curves. See figure 10. For small $\tilde{\ell}$ (*i.e.* $\lesssim 2$), saturation is reached well before we enter the linear phase, so we may expect differences in the saturation time for those cases versus large $\tilde{\ell}$.

It is important to note that our saturation time is a departure from the result of $\tilde{\ell}/2$ for the 1+1 CFT result of ref. [3], reproduced in the holographic thermal quench studies of refs.[8, 20].

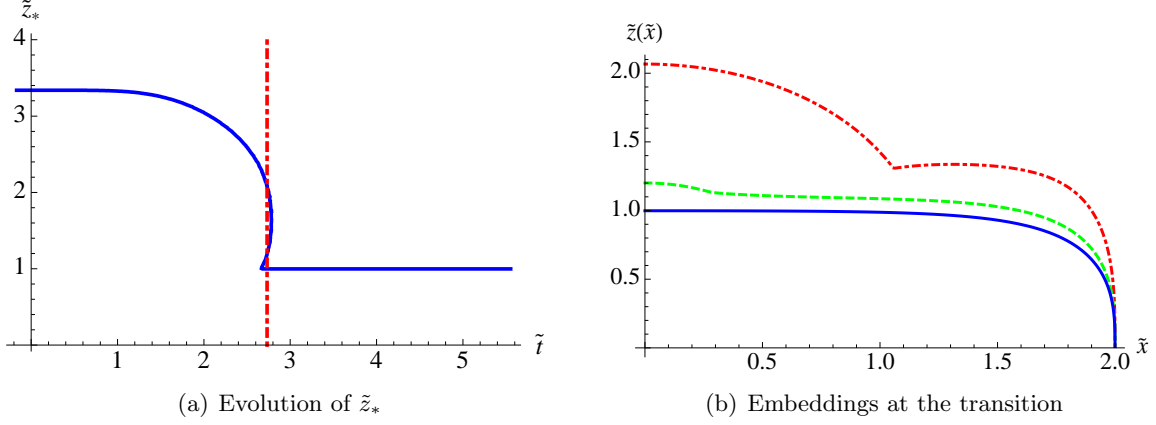


Figure 11: Behavior of \tilde{z}_* for $\tilde{\ell} = 4$ and $\tilde{v}_0 = 0.01$. In (a), the red dashed line is where the transition occurs and the apparent horizon is at $z = 1$. In (b), we display the two embeddings at the transition, where the red, dot-dashed curve corresponds to the embedding with $\tilde{z}_* = 2.0669$, the green, dashed curve corresponds to the embedding with $\tilde{z}_* = 1.2010$, and the blue, solid curve corresponds to the embedding with $\tilde{z}_* = 0.9985$

Note that here the excitations do not necessarily travel a distance of order 2ℓ during this time. Because of the geometry of the strip, some excitations can travel much greater lengths. Therefore, the overall effective speed of saturation of \tilde{s} should be expected to be less than the speed of light, as we have seen in our results for the strip.

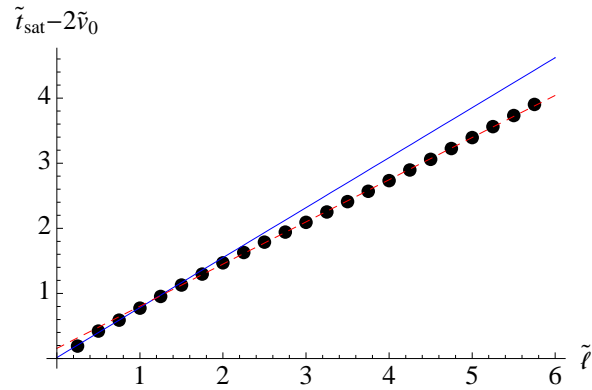


Figure 12: The saturation time as a function of $\tilde{\ell}$ for thermal quench of the strip. The solve of the best fit line for small $\tilde{\ell}$ depicted with the solid blue line is 0.77. The slope of the best fit line for large $\tilde{\ell}$ depicted with the red dashed line is 0.65.

3.2 The Disc

We can perform similar calculations for the disc. The area of the two dimensional surface is given by equation (28), and we define:

$$\tilde{s} = \int_0^{\tilde{\ell}} d\tilde{r} \frac{\tilde{r}}{\tilde{z}(\tilde{r})^2} \sqrt{1 - f(\tilde{v}, \tilde{z})\tilde{v}'(\tilde{r})^2 - 2\tilde{v}'(\tilde{r})\tilde{z}'(\tilde{r})} - \frac{\tilde{\ell}}{\tilde{\epsilon}} + 1 \quad (73)$$

We present some results in figure 13. There are several differences from the strip case. First, we see that the early evolution strongly depends on $\tilde{\ell}$. Once again, this can be understood from the geometry of \mathcal{A} . The region near the boundary of \mathcal{A} has a size that grows with ℓ and so the early evolution of the entanglement should reflect this dependence on geometry. Another key difference from the strip case is that no matter how large $\tilde{\ell}$ is, we do not see the kink in the transition to saturation. In line with our reasoning from the previous section, the saturation value of the entanglement entropy and the rate of approach to saturation increase in lock with $\tilde{\ell}$ (unlike for the strip where the rate was independent of $\tilde{\ell}$) allowing for a smooth evolution towards saturation. Furthermore, we see that the saturation time grows linearly (with a slope of unity) with $\tilde{\ell}$. This fits with the fact that the disc's finite extent in all directions means that there is a maximum travel time for any excitations as a result of the quench to leave \mathcal{A} and contribute to the entanglement entropy. So in this way we recover that the rate of saturation of the entanglement entropy is the speed of light, as was observed in lower dimensions. In this sense, the disc is a more natural generalization of the 1+1 dimensional case than the strip.

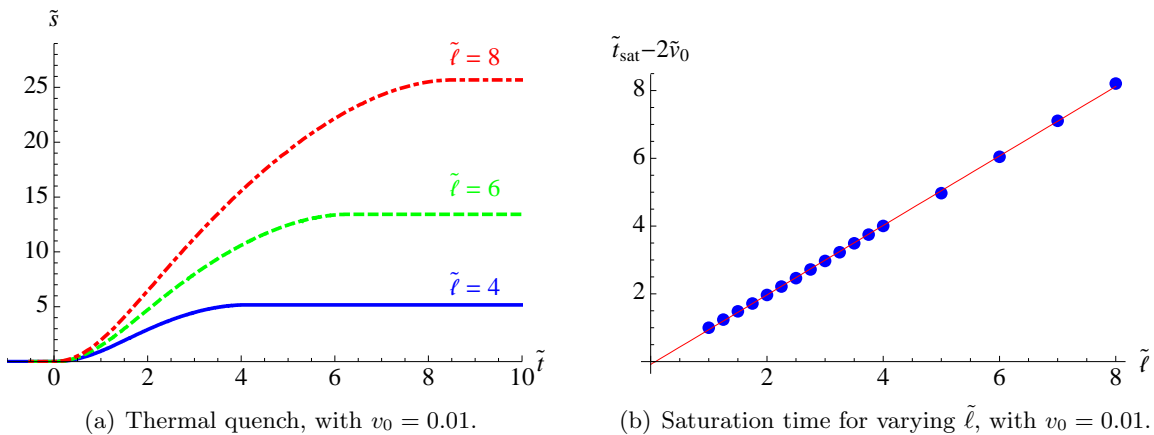


Figure 13: Results for thermal quench with a disk. The slope of the saturation time is almost exactly unity.

4 The Electromagnetic Quench

It is possible to cleanly study an entirely different type of quench in this system. This non-thermal quench is achieved by turning on electric and magnetic sources of the theory. We choose the system to be entirely non-thermal by approaching the extremal (*i.e.*, zero temperature) black hole solution at late times². The electric components of the background at late times can be read off as non-zero charge density and chemical potential in the dual 2+1 dimensional field theory[26, 27], whilst the magnetic components represent a background magnetic field[28]. In fact, electric-magnetic duality invariance of our system means that different choices of electric or magnetic sources can be rotated into each other, and we will often think of the system as undergoing a purely magnetic quench for convenience, but admixtures of electric (chemical potential) and magnetic (background field) quenches are captured by all of our results.

The collapsing charged geometry has a metric similar to the extremal AdS₄ metric from the section 2.3.3, but with the function f now taken to be:

$$f(v, z) = 1 - 4 \left(\frac{z}{z_0(v)} \right)^3 + 3 \left(\frac{z}{z_0(v)} \right)^4, \quad (74)$$

taking:

$$q_e(v)^2 + q_m(v)^2 = \frac{3R^6}{z_0(v)^4}, \quad m(v) = \frac{2R^4}{z_0(v)^3}. \quad (75)$$

We use the same quench profile for $z_0(v)$ as that given in equation (67). Note that here z_∞ sets the final strength of the magnetic field (in the duality frame where we choose everything to be magnetic).

4.1 The Strip

We proceed in a similar fashion as in the case of the thermal quench. The area is given by equation (71), and we define the finite entanglement entropy \tilde{s} by equation (72). Let us consider first the effect of quench speed, set by \tilde{v}_0 . We present an example in figure 14. As with the thermal quench, it seems the general behavior of the entanglement entropy for small enough $\tilde{\ell}$ is qualitatively universal. When \tilde{v}_0 is small enough, it appears that the rise time to linear behavior does not depend on \tilde{v}_0 , suggesting that there is an intrinsic time scale for the dual plasma to react to changes in the medium, as in the case of one dimension fewer [20]. It is interesting to note, however, that the time scale in the current system appears to be much smaller than that of ref.[20]. As in the thermal case, for large \tilde{v}_0 , the evolution of the entropy appears to follow the evolution of

²Since the extremal solution is a highly degenerate point in the space of black hole solutions, it is clear that forming one by collapse is a delicate process. However, it is possible, at least formally. It turns out that the novel physics that we observe in this system does not appear to depend upon the details of the process of formation.

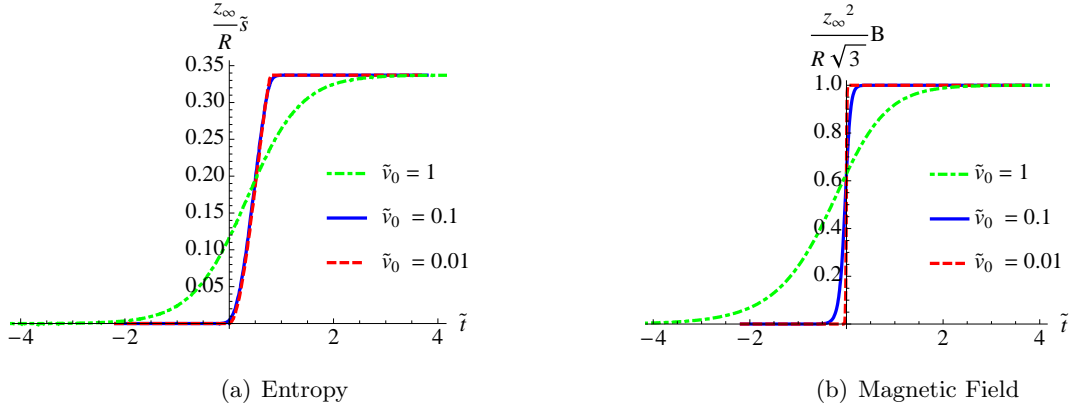


Figure 14: The entropy and magnetic field for $\tilde{\ell} = 1$.

the quench rather closely. We consider the effect of strip size $\tilde{\ell}$, presenting some results in figure 15. The early time evolution is independent of $\tilde{\ell}$ just as we saw for the thermal case. Furthermore, for large enough $\tilde{\ell}$, there is again the appearance of a swallow tail, controlling the rapid flattening out to saturation. The resulting kink in the entanglement entropy has a similar origin to that discussed in section 3.1, although in this case the situation is more severe since the rate of approach is slowed down by the logarithmic behavior. An increase in $\tilde{\ell}$ give an increases in size for the swallow tail,

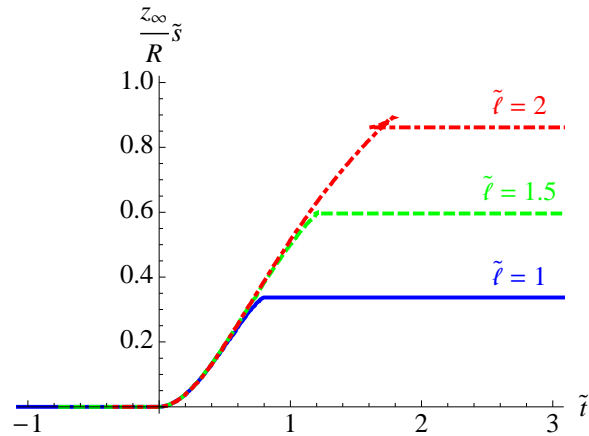


Figure 15: The entropy for various values of $\tilde{\ell}$ and $\tilde{v}_0 = 0.01$.

and eventually the transition occurs even before the beginning of the swallow tail region is ever reached. See an example in figure 16.

A new important feature is a departure from the linear behavior of the evolution to a logarithmic growth. This behavior is inherited from the logarithmic behaviour we saw in the static extremal case in section 2.3.3, which has its origin in the double zero at the horizon. On the dual

field theory side, this means significantly new behaviour for the excitations as they propagate after the quench. Presumably, the charged excitations are slowed down by electromagnetic interactions, either from screening in the presence of non-zero charge density or due to propagation in the background magnetic field³.

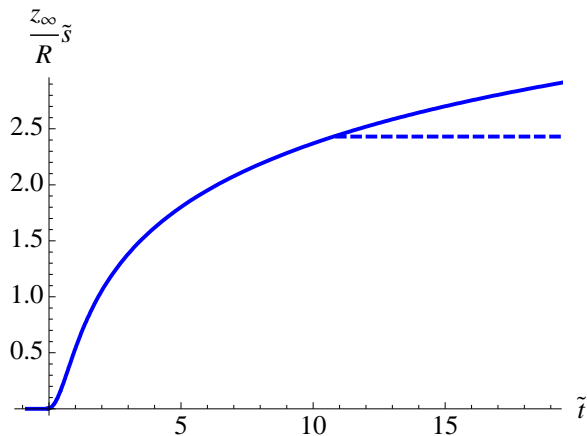


Figure 16: The entropy for $\tilde{\ell} = 5$ and $\tilde{v}_0 = 0.1$. The intermediate time behavior of the area is well approximated by $\ln \tilde{t}$. The dashed line corresponds to the second embedding to which the system transitions, showing entanglement saturation.

We can study how the saturation time t_{sat} depends on $\tilde{\ell}$. We present these results in figure 17. We find that the slope of the line near $\tilde{\ell} = 0$ is approximately 0.77 (note again that the slope depends slightly on how one decides to calculate t_{sat} because of the roundedness of the solution before it saturates), which matches our earlier result for the thermal quench. Upon reaching the point where the jump between embeddings starts to occur, the growth in \tilde{t}_{sat} appears to be well fitted with an exponential from that point onwards (to be expected from the logarithmic growth of the area with time that we commented on earlier).

4.2 The Disc

We proceed in a similar fashion as in the case of the thermal quench. The area is given by equation (28), and we define the finite entanglement entropy \tilde{s} by equation (73). We present some results in figure 18. Again, the early evolution has strong $\tilde{\ell}$ dependence in a manner attributable to the disc geometry. Also present is the logarithmic evolution, arising from the near horizon region of the geometry. Furthermore, for large enough $\tilde{\ell}$, there is an appearance of the swallow tail. Recall that this was absent for the thermal quench for the disc. In line with the discussion in section 3.1,

³Logarithm growth of entanglement entropy has been observed in (1+1)-dimensional systems quenched with an external field (see *e.g.* ref.[29]). It would be interesting to explore the possibility of a connection to our results.

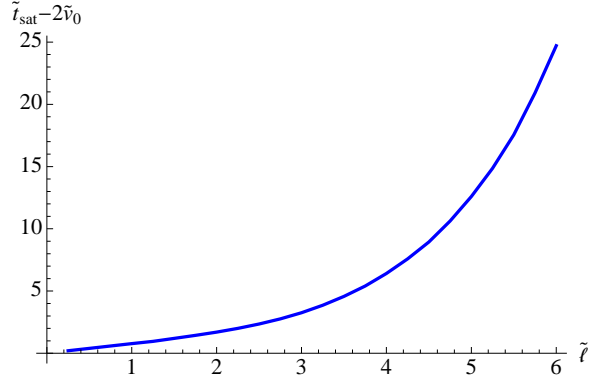


Figure 17: The saturation time as a function of $\tilde{\ell}$ for $\tilde{v}_0 = 0.01$. The slope near $\tilde{\ell} = 0$ is approximately 0.77.

its appearance here is due to the slowing (as opposed to increasing in the thermal case) rate of approach to saturation with increasing $\tilde{\ell}$ due to the logarithmic behavior.

5 Conclusions

We have studied two types of quench for the (2+1)-dimensional theory dual to AdS₄, computing the evolution of the entanglement entropy for an infinite strip region and a round disc region. Our quenches were a thermal quench dual to a shell of uncharged matter (which forms a Schwarzschild black hole) and a non-thermal quench, formed from a shell of charged matter (which we tuned to form an extremal (*i.e.*, zero temperature) dyonic black hole).

We observed several interesting phenomena. The results for the disc, for the thermal quench, provided the most direct analogue of earlier observed results from (1+1) dimensions[3, 8, 20]: There was linear growth in time of the entanglement entropy on its way to saturation, with a slope consistent with the interpretation that the quanta responsible for entanglement were propagating with the speed of light. The strip deviated from this in two ways. The first, that the effective growth rate (while still linear) was slower than the disc’s was naturally attributable to the semi-infinite geometry of the strip. The second was more surprising. For large enough strip size there was a kink in the entropy–time curve corresponding to a rapid turnover at saturation. The source of this on the geometry side is quite natural (it is due to the availability of multiple branches of candidate minimal surface solutions, forming a swallow tail shape — there is a jump from one branch to another at late enough times), but it would be interesting to understand its origins on the field theory side. The kink suggests a modification of the picture proposed in ref. [3], whereby not just entangled pairs contribute to the entanglement entropy. (Note that it is probable that such a kink gets softened beyond the supergravity approximation.)

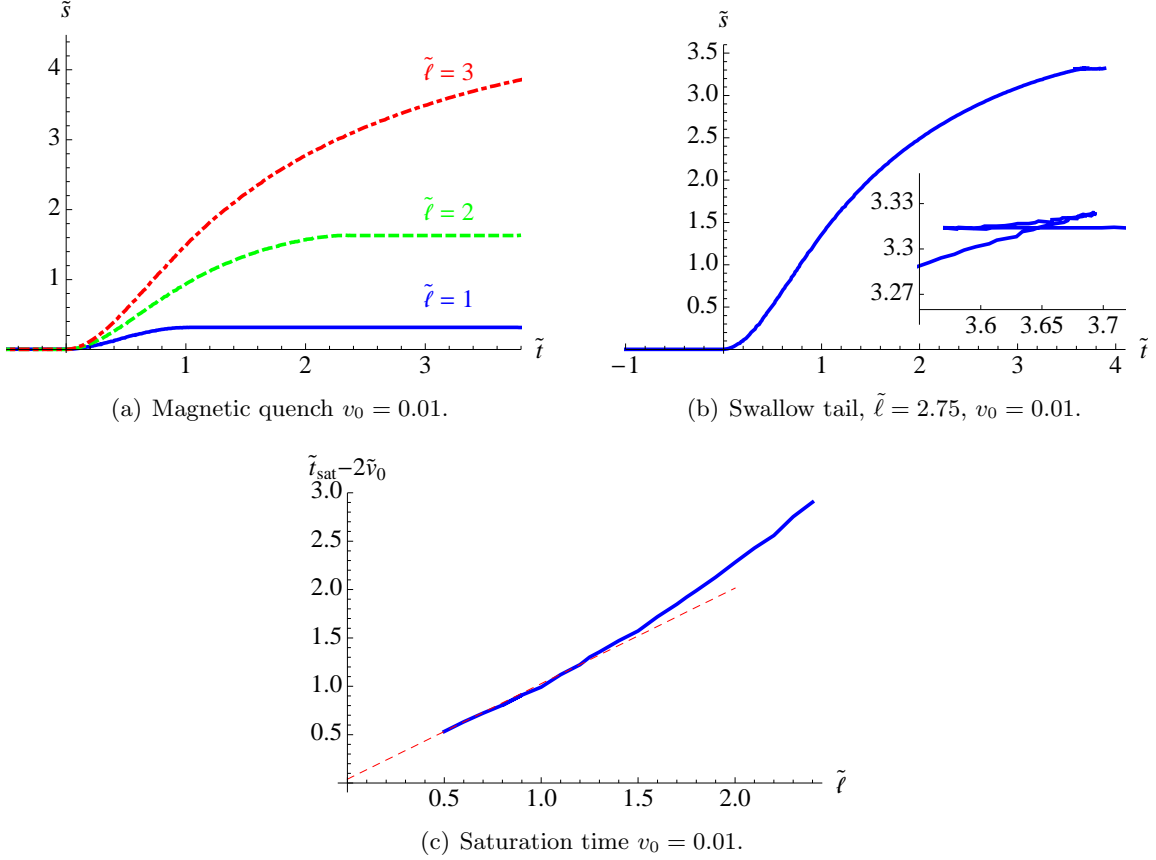


Figure 18: Results for magnetic quench with a disc. The slope of the saturation time for small $\tilde{\ell}$ is almost exactly unity.

The kink is also present for both the disc and the strip for the electromagnetic quench. One of the features of our novel quench is that the entanglement entropy grows only logarithmically with time, a feature that may be due (on the field theory side) to screening effects for the charged quanta. It is interesting that kinks appear when the effective propagation speed contributing to the entanglement entropy growth is subluminal for both thermal and electromagnetic cases, being absent for the thermal quench disc case. We do not know if this is a coincidence, but are encouraged to pursue further study of this issue.

In interpreting our results, we have assumed that the prescription to calculate the entanglement entropy is correct. New features like the kink have been discussed from this point of view (see section 3.1). We recognize that, until a better understanding of the prescription is obtained, it is possible that the kink may be interpreted as pathological, indicating a breakdown of the prescription to calculate the entanglement entropy for rapid quenches and large system size.

The logarithmic growth is again something that would be interesting to understand further on the field theory side. On the gravity side it comes from surfaces that probe near the extremal horizon, which has a double zero in the metric function. A throat opens up at the horizon, producing a smooth geometry that is $\text{AdS}_2 \times \mathbb{R}^2$. It is tempting to speculate that for our electromagnetic quench, the growth of entropy in the intermediate region might be captured by an effective lower dimensional theory captured by AdS_2 physics, as has been shown to happen for aspects of the physics of studying Fermi surfaces holographically in a related context[30, 31].

Acknowledgments

TA would like to thank Stephan Haas for sparking our interest in this work and for various useful discussions. TA and CVJ would also like to thank Hubert Saleur, Silvano Garnerone, Rob Myers and Mukund Rangamani for useful discussions and comments as well as Esperanza Lopez for clarifications about aspects of ref.[20]. This work was supported by the US Department of Energy.

Appendix: A Note on Unitarity of Quench Evolution

In order to show that the evolution of the quench and subsequent relaxation process is unitary, we would like to show that throughout the evolution the following condition is satisfied:

$$S_{\mathcal{A}} = S_{\mathcal{B}} . \tag{76}$$

It is useful to start with some static examples before considering an evolving background. Let us begin with the case of pure AdS_4 . To compute $S_{\mathcal{B}}$, there are two possible surfaces to consider [12], which we depict in figure 19. The embedding in figure 19(a) can be shown to be divergent by first considering it to be a sum of two finite intervals and then sending the outer edges of the intervals to infinity. The embedding in figure 19(b) has a piece that gives $S_{\mathcal{A}}$ and the contribution from the piece at $z = \infty$ is zero. Therefore, we find that AdS_4 corresponds to a pure state.

Let us now consider a static Schwarzschild black hole. Repeating the calculation described above, we find that the second piece of figure 19(b) must lie not at $z = \infty$ but at $z = z_0$, the horizon. Because of this fact, its contribution gives a non-zero value; in fact it gives an entropy of:

$$S_{\mathcal{B}} = S_{\mathcal{A}} + \frac{1}{4G_{\text{N}}} \left(\frac{R^2}{z_0^2} \int dx dy \right) = S_{\mathcal{A}} + \frac{\text{Area}(\text{E.H.})}{4G_{\text{N}}} , \tag{77}$$

where $\text{Area}(\text{E.H.})$ is the area of the event horizon. Therefore, we find that $S_{\mathcal{B}} \neq S_{\mathcal{A}}$, and so the system is not in a pure state. Therefore, any static solution with an event horizon corresponds to a mixed state (see e.g. ref.[32]).

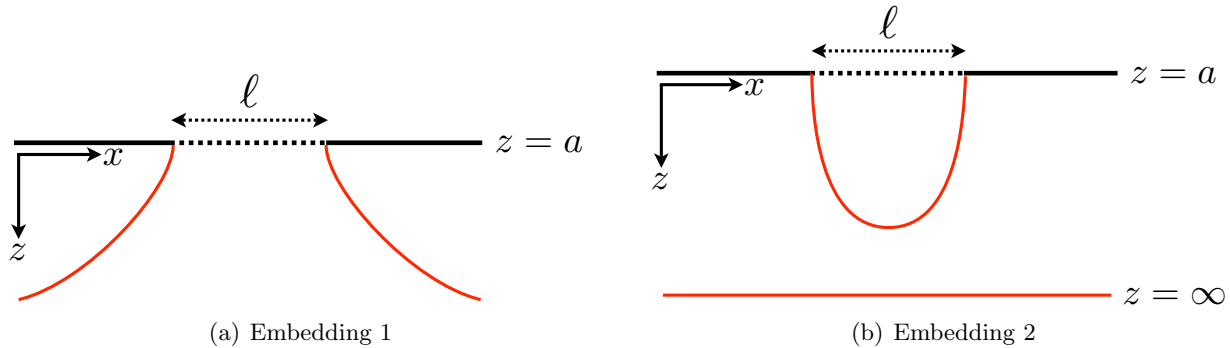


Figure 19: Diagrams of the two types of embeddings to calculate entanglement entropy of \mathcal{B} .

So let us now consider our evolving metric. If we consider a solution that corresponds to the embedding of figure 19(b), a solution to the equations of motion for the second disjoint piece is to simply have:

$$z(x) = \infty, \quad v(x) = -\infty. \quad (78)$$

We note that for $v(x) = -\infty$, our metric does not have a singularity at $z(x) = \infty$, so there is no danger for the solution to lie there. In particular, this solution is (in a sense) simply the solution that we would get for AdS_4 and gives zero contribution to the entropy. The first piece will give us the entropy of \mathcal{A} . Therefore, for the evolving case, we find that we have:

$$S_{\mathcal{A}} = S_{\mathcal{B}}, \quad \forall t \quad (79)$$

Note that this only works because we are assuming the second piece remains static in the sense that it remains at $v = -\infty$ whereas the other piece evolves. Therefore, with this in mind, we find that the evolution is unitary.

References

- [1] P. Calabrese and J. Cardy, “Entanglement entropy and conformal field theory,” *Journal of Physics A: Mathematical and Theoretical* **42** (2009) no. 50, 504005, [arXiv:0905.4013](#) [[cond-mat](#)].
- [2] M. Srednicki, “Entropy and area,” *Phys. Rev. Lett.* **71** (1993) 666–669, [arXiv:hep-th/9303048](#).
- [3] P. Calabrese and J. Cardy, “Evolution of entanglement entropy in one-dimensional systems,” *Journal of Statistical Mechanics: Theory and Experiment* **2005** (2005) no. 04, P04010, [arXiv:cond-mat/0503393](#).

- [4] J. M. Maldacena, “The large n limit of superconformal field theories and supergravity,” *Adv. Theor. Math. Phys.* **2** (1998) 231–252, [hep-th/9711200](#).
- [5] E. Witten, “Anti-de sitter space and holography,” *Adv. Theor. Math. Phys.* **2** (1998) 253–291, [hep-th/9802150](#).
- [6] S. S. Gubser, I. R. Klebanov, and A. M. Polyakov, “Gauge theory correlators from non-critical string theory,” *Phys. Lett.* **B428** (1998) 105–114, [hep-th/9802109](#).
- [7] S. Ryu and T. Takayanagi, “Aspects of holographic entanglement entropy,” *JHEP* **08** (2006) 045, [arXiv:hep-th/0605073](#).
- [8] V. E. Hubeny, M. Rangamani, and T. Takayanagi, “A covariant holographic entanglement entropy proposal,” *JHEP* **07** (2007) 062, [arXiv:0705.0016](#) [[hep-th](#)].
- [9] T. Nishioka, S. Ryu, and T. Takayanagi, “Holographic Entanglement Entropy: An Overview,” *J. Phys.* **A42** (2009) 504008, [arXiv:0905.0932](#) [[hep-th](#)].
- [10] O. Aharony, S. S. Gubser, J. M. Maldacena, H. Ooguri, and Y. Oz, “Large n field theories, string theory and gravity,” *Phys. Rept.* **323** (2000) 183–386, [hep-th/9905111](#).
- [11] D. V. Fursaev, “Proof of the holographic formula for entanglement entropy,” *JHEP* **09** (2006) 018, [arXiv:hep-th/0606184](#).
- [12] M. Headrick, “Entanglement Renyi entropies in holographic theories,” [arXiv:1006.0047](#) [[hep-th](#)].
- [13] S. N. Solodukhin, “Entanglement entropy of black holes and AdS/CFT correspondence,” *Phys. Rev. Lett.* **97** (2006) 201601, [arXiv:hep-th/0606205](#).
- [14] T. Hirata and T. Takayanagi, “AdS/CFT and strong subadditivity of entanglement entropy,” *JHEP* **02** (2007) 042, [arXiv:hep-th/0608213](#).
- [15] T. Nishioka and T. Takayanagi, “AdS bubbles, entropy and closed string tachyons,” *JHEP* **01** (2007) 090, [arXiv:hep-th/0611035](#).
- [16] M. Headrick and T. Takayanagi, “A holographic proof of the strong subadditivity of entanglement entropy,” *Phys. Rev.* **D76** (2007) 106013, [arXiv:0704.3719](#) [[hep-th](#)].
- [17] S. N. Solodukhin, “Entanglement entropy, conformal invariance and extrinsic geometry,” *Phys. Lett.* **B665** (2008) 305–309, [arXiv:0802.3117](#) [[hep-th](#)].

- [18] H. Casini, M. Huerta, and L. Leitaó, “Entanglement entropy for a Dirac fermion in three dimensions: vertex contribution,” *Nucl. Phys.* **B814** (2009) 594–609, [arXiv:0811.1968 \[hep-th\]](#).
- [19] H. Casini, M. Huerta, and R. C. Myers, “Towards a derivation of holographic entanglement entropy,” [arXiv:1102.0440 \[hep-th\]](#).
- [20] J. Abajo-Arastia, J. Aparicio, and E. Lopez, “Holographic Evolution of Entanglement Entropy,” [arXiv:1006.4090 \[hep-th\]](#).
- [21] E. Witten, “Anti-de sitter space, thermal phase transition, and confinement in gauge theories,” *Adv. Theor. Math. Phys.* **2** (1998) 505–532, [hep-th/9803131](#).
- [22] A. Chamorro and K. S. Virbhadra, “Radiating dyon solution in Einstein-Maxwell theory,” [arXiv:hep-th/9406148](#).
- [23] P. Vaidya, “The External Field of a Radiating Star in General Relativity,” *Curr. Sci.* **12** (1943) 183.
- [24] P. Vaidya, “The Gravitational Field of a Radiating Star,” *Pro. Indian Acad. A.* **33** (1951) 264.
- [25] S. R. Das, T. Nishioka, and T. Takayanagi, “Probe Branes, Time-dependent Couplings and Thermalization in AdS/CFT,” *JHEP* **07** (2010) 071, [arXiv:1005.3348 \[hep-th\]](#).
- [26] A. Chamblin, R. Emparan, C. V. Johnson, and R. C. Myers, “Charged AdS black holes and catastrophic holography,” *Phys. Rev.* **D60** (1999) 064018, [hep-th/9902170](#).
- [27] A. Chamblin, R. Emparan, C. V. Johnson, and R. C. Myers, “Holography, thermodynamics and fluctuations of charged ads black holes,” *Phys. Rev.* **D60** (1999) 104026, [hep-th/9904197](#).
- [28] S. A. Hartnoll and P. Kovtun, “Hall conductivity from dyonic black holes,” *Phys. Rev.* **D76** (2007) 066001, [arXiv:0704.1160 \[hep-th\]](#).
- [29] V. Eisler and I. Peschel, “Evolution of entanglement after a local quench,” *Journal of Statistical Mechanics: Theory and Experiment* **2007** (2007) no. 06, P06005.
- [30] T. Faulkner, H. Liu, J. McGreevy, and D. Vegh, “Emergent quantum criticality, Fermi surfaces, and AdS2,” [arXiv:0907.2694 \[hep-th\]](#).

- [31] T. Faulkner and J. Polchinski, “Semi-Holographic Fermi Liquids,” [arXiv:1001.5049](#) [hep-th].
- [32] R. C. Myers, “Pure states don’t wear black,” *Gen. Rel. Grav.* **29** (1997) 1217–1222, [arXiv:gr-qc/9705065](#).